Monitoring of Receptor Dimerization Using Plasmonic Coupling of Gold Nanoparticles

Matthew J. Crow,[†] Kevin Seekell,[†] Julie H. Ostrander,[‡] and Adam Wax[†,*]

[†]Department of Biomedical Engineering, Duke University, Durham, North Carolina 27708, United States, and [‡]Department of Medicine, University of Minnesota Cancer Center, Minneapolis, Minnesota 55455, United States

ABSTRACT 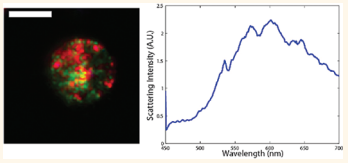

The dimerization of receptors on the cell membrane is an important step in the activation of cell signaling pathways. Several methods exist for observing receptor dimerization, including coimmunoprecipitation, chemical cross-linking, and fluorescence resonance energy transfer (FRET). These techniques are limited in that only FRET is appropriate for live cells, but even that method suffers from photobleaching and bleed-through effects. In this study, we implement an alternative method for the targeting of HER-2 homodimer formation based on the plasmonic coupling of gold nanoparticles functionalized with HER-2 Ab. In the presented studies, SK-BR-3 cells, known to overexpress HER-2, are labeled with these nanoparticles and receptor colocalization is observed using plasmonic coupling. HER-2 targeted nanoparticles bound to these cells exhibit a peak resonance that is significantly red-shifted relative to those bound to similar receptors on A549 cells, which have significantly lower levels of HER-2 expression. This significant red shift indicates plasmonic coupling is occurring and points to a new avenue for assessing dimerization by monitoring their colocalization. To determine that dimerization is occurring, the refractive index of the nanoenvironment of the labels is assessed using a theoretical analysis based on the Mie coated sphere model. The results indicate scattering by single, isolated nanoparticles for the low HER-2 expressing A549 cell line, but the scattering observed for the HER-2 overexpressing SK-BR-3 cell line may only be explained by plasmonic-coupling of proximal nanoparticle pairs. To validate the conformation of nanoparticles bound to HER-2 receptors undergoing dimerization, discrete dipole approximation (DDA) models are used to assess spectra of scattering by coupled nanoparticles. Comparison of the experimental results with theoretical models indicates that NP dimers are formed for the labeling of SK-BR-3 cells, suggesting that receptor dimerization has been observed.

KEYWORDS: nanoparticles · plasmonic coupling · receptor dimerization · light scattering

Understanding the dynamics of receptors in the cell membrane can be important in identifying the mechanisms that regulate various types of essential cell activities. For example, the ErbB receptor family consists of four structurally similar receptor tyrosine kinases, including epidermal growth factor receptor (EGFR/ErbB-1), human epidermal growth factor receptor 2 (HER-2/ErbB-2), ErbB-3, and ErbB-4. These receptors are responsible for the regulation of multiple signaling pathways that control cell proliferation, differentiation, survival, mobility, and adhesion.[1,2] Upon growth factor ligand binding, these receptors undergo a conformational change and become activated receptors, forming either homodimers or heterodimers, depending on several factors. In this study, we focus on HER-2 which primarily serves as a heterodimeric partner for other members of the ErbB family because it always is in an active confirmation and does not bind growth factor ligands.[2,3] However, when cells express high levels of HER-2, the receptor undergoes constitutive homodimerization.[1,4] The ability to monitor the dimerization behavior of HER-2 may provide a means to illuminate the mechanisms by which these different receptor signaling pathways interact, with implications toward the development of new drugs and therapies for the treatment of various cancers, including breast and ovarian.[1]

Several methods exist for the observation of receptor dimerization, including coimmunoprecipitation, chemical cross-linking, and fluorescence resonance energy transfer (FRET), but each has its own limitations which require consideration.[5] Co-immunoprecipitation, which entails detergent solubilization,[6] can lead to aggregation of hydrophobic proteins, such as HER-2.[7] In addition, both coimmunoprecipitation and chemical cross-linking techniques disrupt the cell,[8] preventing *in vitro* live cell monitoring of dimerization behavior. While FRET allows for *in vitro* live cell measurement of distance between proteins, the approach can be limited due to factors such as photobleaching, autofluorescence, and spectral bleed-through.[9] An alternative approach can be found in bioluminescence resonance energy transfer (BRET), although, since the

* Address correspondence to a.wax@duke.edu.

Received for review April 20, 2011 and accepted October 14, 2011.

Published online October 14, 2011
10.1021/nn201451c

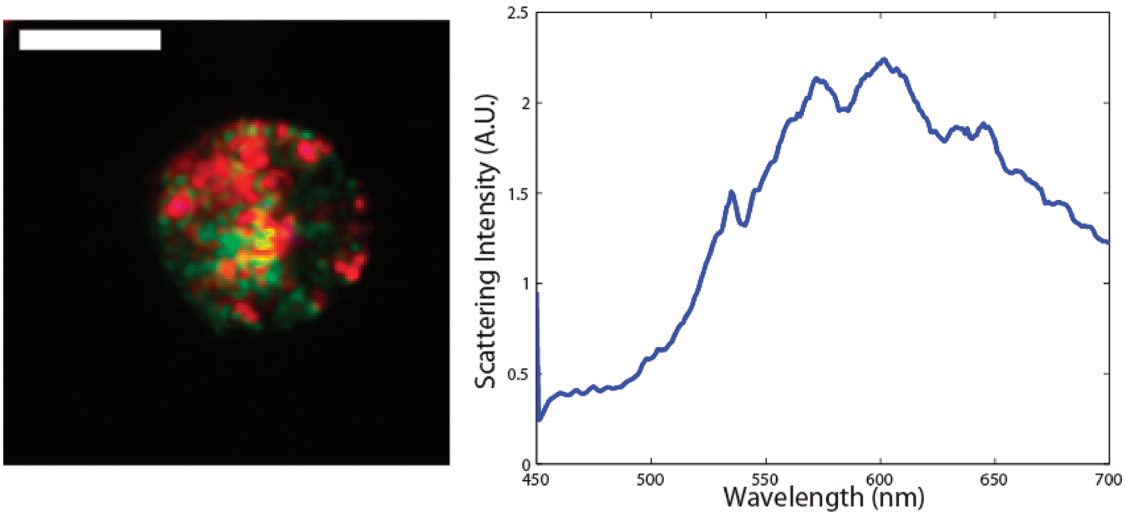

Figure 1. Representative image (left) and spectrum (right) of SK-BR-3 cell bound with HER-2 Ab immunolabeled 60 nm gold NPs. The peak wavelength of the scatter is at 595.1 ± 26.0 nm (scale bar =10 μm).

technique lacks high spatial resolution, application of BRET to single cells remains of limited utility.[10]

Here, we propose the use of noble metal plasmonic nanoparticles (NPs) as an alternative method of monitoring receptor interactions. These particles exhibit surface plasmon resonances, characterized by strongly enhancing scattering and absorption at selected wavelengths, providing a means for obtaining high imaging contrast. The peak resonance of the particles is dependent on several factors including, size, shape, and composition. In addition, local refractive index greatly influences the peak wavelength of the resonance, providing a unique tool for the investigation of dielectric environments on the nanometer scale, including cellular environments.[11] Conjugation of the NPs to antibodies provides a simple method of targeting receptors that are commonly overexpressed in various cancer cell phenotypes. In addition to their dielectric environment, plasmonic coupling of proximal NPs also plays a role in their scattering and absorption properties. Plasmons between NP pairs and clusters interact, resulting in a red shift of the peak resonant wavelength and a strong increase in the amount of scattered and absorbed light from the pair, relative to either particle individually. Plasmonic coupling has been shown to be a powerful tool in many biological research applications. The enhanced scattering efficiency significantly increases biomarker contrast in molecular imaging of various sample types, including animal models of carcinogenesis.[12] The red-shift due to plasmonic coupling has been exploited to enable dynamic studies of EGFR internalization[13] and to provide contrast for photoacoustic imaging.[14] Additionally, the extent of the red shift decays approximately exponentially with increasing interparticle separation .[15] This relationship allows for "molecular ruler" applications using NP dimers, including the observation of single DNA hybridization events.[16,17] Plasmonic NPs can even be used for measurements above the limit of FRET (typically 10 nm[18]), but still under the diffraction limit of optical microscopy.[19] Unfortunately, coupling also has the drawback of complicating interpretation of spectral data in dielectric sensing applications of NPs. In the presence of proximal NPs, it may not be clear whether the red shift is due to coupling or simply an increase in the local cellular refractive index.

In this study, we investigate the use of plasmonic NPs for the observation of HER-2 dimer pairs. Analysis of scattering by NPs bound to two different cell lines with different levels of HER-2 expression reveal that the calculated refractive index of the nanoparticle environment may be attributed either to the dielectric environment or plasmonic coupling, depending on the red-shift of the peak scattering wavelength. Validation of the analysis is provided by using discrete dipole approximation (DDA) simulations of proximal NP pairs to determine the predicted conformation of the particles and assess if dimerization has occurred.

RESULTS AND DISCUSSION

Cell Labeling Experiments. Scattering spectra were acquired from *in vitro* cultures of SK-BR-3 (HER-2 ++) and A549 (HER-2+) cells using the microspectroscopy system[20] and averaged over the entire cell. Summed spectra for each cell were fit to a Gaussian distribution, which provides an average peak scattering wavelength for this label when bound. For the typical data in Figure 1, the scattering peak for SK-BR-3 cells was found to be 595.1 ± 26.0 nm (average of N = 147 measurements across the individual cell). The peak scattering wavelengths taken for 122 cells were binned to create a histogram for each cell line which was in turn fit to a Gaussian distribution. The histogram fit for the SK-BR-3 cells indicated a peak wavelength of 587.0 ± 11.9 nm (N = 122 cells), as shown in Figure 2. Following a similar

round of imaging experiments, scattering data were acquired for A549 cells labeled with HER-2 Ab gold nanospheres (Figure 3). For this typical data, the scattering peak was observed at 555.1 ± 20.1 nm (average of $N = 126$ measurements across individual cell). Note the green appearance of this cell in the color image, compared with the reddish appearance of the SK-BR-3 cell in Figure 1. Upon peak scattering wavelengths for 75 cells were binned to create a histogram (Figure 4) with a peak of 551.4 ± 8.6 nm.

Demonstration of Molecular Specificity. To confirm that the NPs were targeted to the HER-2 receptor, multiple control experiments were conducted (Figure 5). Control experiments consisted of exposure of HER-2 nonexpressing MDA-MB-468 human breast adenocarcinoma cells to HER-2 Ab NP conjugates,[21−23] HER-2 expressing SK-BR-3 cells exposed to IgG_1 Ab gold NP conjugates, and SK-BR-3 cells not exposed to any NPs. Control experiments all showed negligible increases in scattering demonstrating statistically significant differences in scattering intensity ($p < 0.001$) and thus molecular specificity was confirmed, as in previous applications of these labels.[11,20,24]

Determination of Local Refractive Index (RI). To assess the local nanoenvironment of the nanoparticle labels, a series of characterization steps were required. First, extinction measurements of the uncoated gold spheres suspended in PBS solution were acquired, indicating a peak wavelength of 535.3 ± 0.5 nm. Using the peak wavelength of the extinction measurement and the known RI of the PBS suspension (1.335), Mie theory calculations were used to determine the average NP diameter to be 59.1 ± 0.03 nm, which is in close agreement with the TEM measured value of 61.2 ± 4.3 nm ($N = 183$ NP measurements).[25,26] Second, the antibody layer thickness of HER-2 Ab coated gold NPs was measured using TEM and determined to be 5.2 ± 1.8 nm ($N = 142$ measurements). Using the antibody thickness, in addition to the coated NP extinction peak of 538.7 ± 0.5 nm, as input to a coated sphere Mie theory model enabled determination of the RI of the antibody layer to be 1.43 ± 0.03. For the A549 cells, this information is used to determine the local refractive index surrounding the label. For the mean scattering peak of 551.4 ± 8.6 nm, coated sphere Mie theory models are used to determine that the local refractive index for the gold NP spheres is 1.44 ± 0.03. However, following the same analysis for the SK-BR-3 cells, the mean scattering peak of 587.0 ± 11.9 nm produces a local RI in the volume around the label to be 1.86 when

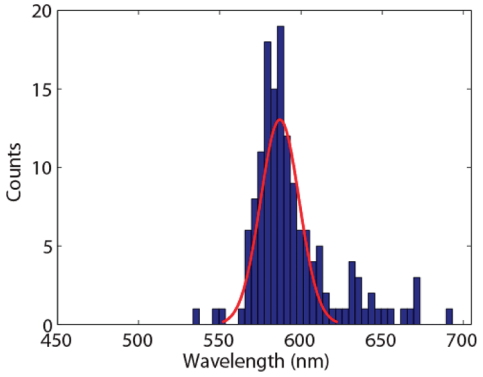

Figure 2. Histogram of peak scattering wavelength of SK-BR-3 cells bound with HER-2 Ab immunolabeled 60 nm gold NPs. Distribution fit has peak wavelength of 587.0 ± 11.9 nm ($N = 122$).

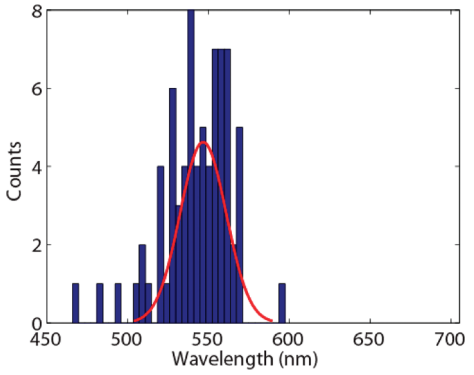

Figure 4. Histogram of peak scattering wavelength for A549 cells exposed to HER-2 Ab immunolabeled 60 nm gold nanospheres. Distribution fit has peak wavelength of of 551.4 ± 8.6 nm ($N = 75$).

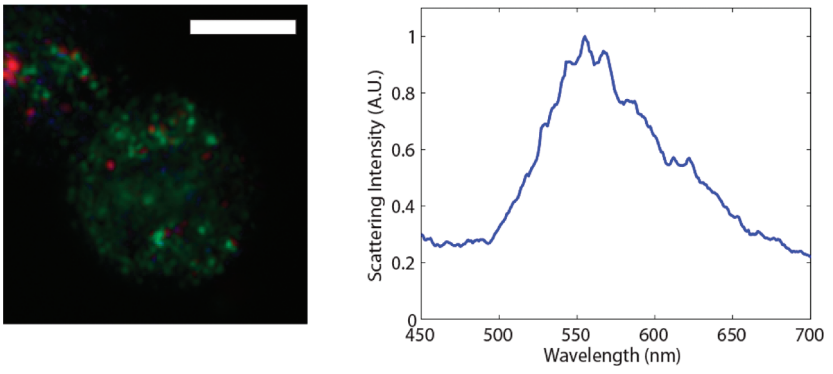

Figure 3. Representative image (left) and spectrum (right) of A549 cell bound with HER-2 Ab immunolabeled 60 nm gold NPs. The peak wavelength of the scatter is at 555.1 ± 20.1 nm (scale bar =10 μm).

analyzed with the coated sphere Mie theory model which does not take plasmonic coupling between the NPs into account. Figure 6 summarizes these analysis steps graphically.

Assessment of NP Conformation and Spacing. To determine the spacing of the bound NPs, a preliminary approximation of the local RI is needed. Here we identify NPs bound to individual HER-2 receptors that are not undergoing dimerization on SK-BR3 cells by using their scattering spectrum. Ideally, the histogram of peak scattering wavelengths (Figure 2) would show a bimodal distribution with one peak for single bound NPs and a second, red-shifted peak for coupled NPs. However, since there is no clearly identifiable second, smaller peak observed in the histogram, we assume that the lowest 5% of peak wavelengths arise from bound receptors which are not undergoing dimerization. These peaks have a mean scattering wavelength of 556.8 ± 13.1 nm (N = 7 cells). Using this assumption, a RI of 1.46 ± 0.07 is determined for the nanoenvironment of NPs bound to cells, which is in reasonable agreement with the RI found for the nanoenvironment of NPs bound to the A549 cells (1.44 ± 0.03).

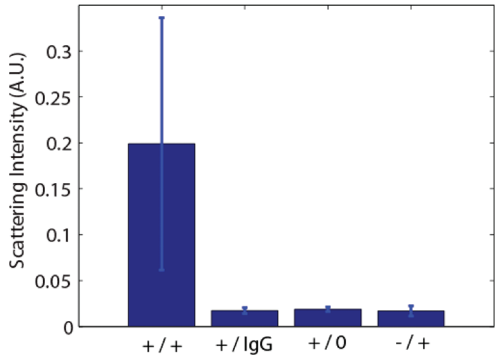

Figure 5. Mean scattering intensity of HER-2 expressing SK-BR-3 cells exposed to HER-2 Ab nanospheres (+/+), SK-BR-3 cells exposed to IgG Ab nanospheres (+/IgG), SK-BR-3 cells unexposed to conjugates, and HER-2 nonexpressing MDA-MB-468 cells exposed to HER-2 Ab nanospheres (−/+).

To evaluate the influence of plasmonic coupling, DDA models representing a proximal pair of two HER-2 antibody-coated gold NPs were used. Validation of this model was presented previously.[27] For the simulations here, the model used two 59.1 nm gold spheres, each possessing distinct core and mantle dielectric constants, and the antibody coating information gained from the above characterization measurements. For two touching, coated NPs, the interparticle separation of the two gold cores consists solely of the summed thicknesses of two 5.2 nm antibody layers, one for each NP, for a total separation of 10.4 nm. The remaining parameters were taken from the above analysis (antibody layer RI = 1.43 ± 0.03, environment RI = 1.46 ± 0.07). The simulation produces a peak wavelength of 582.1 nm, which is in close agreement with the histogram peak observed in the HER-2 Ab SKBR-3 labeling cell experiment.

Models were also computed for the same two gold NPs with the coating thickness varying from 3.4 to 7.0 nm, to account for the standard deviation observed in the TEM measurements. In these cases, the peak scattering is determined to be 592.9 and 570.9 nm, respectively, with the lower bound producing reasonable agreement with the histogram peak. An additional simulation was performed at an interparticle separation of 2 nm. In this case, the peak wavelength is seen to blue shift from 582.1 to 577.1, confirming the trend of the peak shift with NP separation.

DISCUSSION

A state of constitutive homodimerization is expected with SK-BR-3 cells. However, only one distinct peak wavelength distribution was observed from 450–700 nm. The study presented here further investigates whether the distribution could be attributed to scattering by single isolated spheres or if dimer pairs were

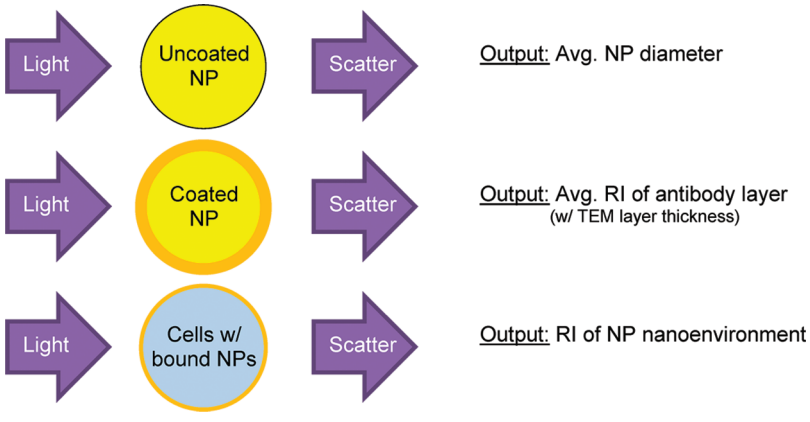

Figure 6. Summary of parameters obtained from scattering measurements. Transmission measurement through uncoated NPs yields average particle diameter. Transmission through coated spheres gives refractive index (RI) of antibody coating by using TEM measurements of coating thickness. With these parameters, the cell scatter measurements give the RI of the NP nanoenvironment.

TABLE 1. Calculation Parameters

input parameter	value
uncoated particle size (TEM)	61.2 ± 4.3 nm
antibody layer thickness (TEM)	5.2 ± 1.8 nm
uncoated colloid extinction peak	535.3 ± 0.5 nm
uncoated particle size (extinction)	59.1 ± 0.03 nm
coated colloid extinction peak	538.69 ± 0.03 nm
antibody layer RI	1.43 ± 0.03
lowest 5% cell bound scatter mean	556.82 ± 13.09 nm
output parameter	**value**
cell bound scatter peak (SK-BR-3)	587.03 ± 11.87 nm
determined RI for bound NPs (SK-BR-3)	1.46 ± 0.07
cell bound scatter peak (A549)	551.4 ± 8.6 nm
determined RI for bound NPs (A549)	1.44 ± 0.03
determined spacing of NPs bound to SK-BR-3 cells	**10.4 nm**

required. On the basis of the peak wavelength of the scattering histogram (Figure 2), of 587.0 ± 11.9 nm (N = 122, SEM = 1.1 nm) for gold NPs bound to the SK-BR-3 cells, in addition to the parameters derived above, the assumption of single sphere scattering produces a local RI in the volume around the label of 1.86 when analyzed with a coated sphere Mie theory model. This RI value is significantly higher than the result found for the NPs bound to A549 cells and represents an unrealistically high dielectric constant for the cell membrane.[25] Thus, for the SK-BR-3 cells the peak scattering distribution of bound NPs must be due to interactions among the NPs themselves, indicating plasmonic coupling.

A previous effort to evaluate receptor dimerization by analyzing NP scattering have shown the ability to assess dynamic changes in spectral scattering due to receptor internalization[13] but did not conduct a quantitative analysis to determine the NP configuration. Our analysis of scattering data using DDA models of coupled spheres indicate that NP dimers with interparticle distances at or slightly below twice the mean antibody layer thickness produce the observed peak wavelength, confirming a conformation in which the two NPs are touching. In fact, the best model fit is produced at a NP spacing of slightly less than twice the antibody layer thickness, suggesting that the antibody layers may even be slightly compressed or overlapped to accommodate the relatively large NP size while bound to receptors with such a small intramolecular spacing. We note that if larger assemblies of NPs were formed, the peak would be further red-shifted, as seen by the few outlying points beyond 600 nm in Figure 3. However, the majority of the peak scattering data falls in a relatively narrow range of wavelengths which can only be explained with dimer pair formation. Following the analysis described by Curry,[28] the uncertainty in the local refractive index of the NP depends on several factors including the thickness and refractive index of the antibody layer. However, the analysis shows that this uncertainty has only a small effect on the ability of NPs to sense their surrounding via plasmon resonance shift such that even large changes in a parameter, such as the TEM-measured layer thickness, would not reduce the cellular refractive index to a value that could be explained without plasmonic coupling.

The HER-2 antibody and SKBR3 cell line used in these experiments were specifically chosen to ensure binding of the conjugates to receptors that are undergoing homodimerization and subsequent receptor-mediated endocytosis. First, the particular clone of HER-2 monoclonal antibody (N12) implemented has previously been shown to promote receptor internalization through accelerated homodimerization.[29,30] Second, the SK-BR-3 cell line used here overexpresses HER-2 at levels that result in constitutive homodimerization.[1,29] Evaluation of dimerization by FRET methods further confirms homodimer formation in SK-BR-3 cells.[31] In comparison, the A549 cells exhibit 10× lower levels of HER-2 expression and thus homodimerization is not expected. Indeed, the analysis of the scattering by NPs bound to HER-2 receptors on the A549 cells do not indicate that plasmonic coupling is occurring. These previous studies can be used to place the results seen here in context, confirming that the scattering profile is due to plasmonic coupling between conjugates bound to two proximal receptors comprising a dimer pair.

A key assumption in this analysis is the use of a RI of 1.46 ± 0.07 for the nanoenvironment of NPs bound to cells. This value was determined by analysis of the peak scattering wavelengths from the lowest 5% in the scattering histogram (Figure 2). This value is in good agreement with values expected for NPs in close proximity to the cell membrane, which typically has RI values ranging from 1.46 to 1.60,[32−35] and with the RI found for the nanoenvironment of NPs bound to A549 cells. The determined RIs and corresponding uncertainties are calculated using the methods described by Curry *et al.*[11] The large uncertainty is attributed to the low sample size when the histogram is narrowed to only the lowest 5% of peak scattering wavelengths. In a previous study by our group,[36] 60 nm gold NPs immunolabeled with anti-EGFR bound to A431 cells, known to overexpress EGFR, were observed with dark-field microspectroscopy, similarly to the current study. A histogram of peak scattering wavelength, centered at 564.8 ± 5.0 nm was found in that study, indicating an average local RI of 1.53 ± 0.02 in the volume surrounding the particle. These experiments showed minimal plasmonic coupling with the same NP and same labeling density used here, but an alternative receptor target. The variation between these previous results and those presented here suggests that the analysis cannot simply take the RI value of the nanoenvironment from the results for the A549 cells.

A previous study has shown that HER-2 homodimers in SK-BR-3 cells have receptor separations of approximately 6.29 nm using FRET techniques.[37] At this spacing, if both proximal receptors are each bound to separate 60 nm diameter NPs, the two labeled biomarkers would necessarily come in contact during dimerization, with an interparticle separation dependent on the coated antibody layer thickness, resulting in a large, easily distinguishable redshift, as seen here. The analysis presented here uses the RI of the cell membrane environment in conjunction with DDA models of plasmonic coupling to attribute the redshifted peak to receptor dimerization.

The analysis presented here provides significant evidence that the red shift of the peak scattering wavelength observed in this study is due to plasmonic coupling and not simply an increased dielectric environment. However, in situations where these two effects do not produce such clear differences in scattering peak wavelength, it may not be possible to separate the two using only the analysis method presented here. Instead, we have developed an alternative technique based on polarization mapping to assess anisotropy in the plasmon resonance. Anisotropic NP targets scatter light according to both their transverse and longitudinal aggregate excitation modes.[38] For example, scattering spectra of gold nanorods contain two distinct peaks associated with the excitation of the mode associated with each dimension, where the longer wavelength peak corresponds to the longer axis. Using polarization, one can selectively excite the mode associated with a single nanorod dimension, resulting in only one distinct scattering peak for each mode.[39] We have demonstrated the ability to use polarization mapping to isolate plasmonic coupling modes by observing pairs of NPs under various interparticle separations.[27] In these experiments, we found that upon orienting the incident polarization along the long axis of the pair, the scattering peak was red-shifted depending on the particle separation. Comparison of the scattering spectra with the corresponding theoretical scattering efficiencies from DDA models under parallel and orthogonal polarization orientations, showed that the plasmonic coupling of two NPs is primarily dependent on excitation of the longitudinal mode parallel to the long pair axis. Polarization control therefore presents a means to isolate the two orthogonal excitation modes, and thus discern the dielectric environment from plasmonic coupling in situations where the degree of plasmonic coupling is not as obvious as that in the case presented here. Further studies which combine the analytical method presented here with polarization mapping measurements will provide insight into the colocalization of cell surface receptors.

CONCLUSION

In summary, we have demonstrated a plasmonic method for the observation of receptor dimerization. A novel HER-2 Ab nanoparticle conjugate was developed for this work and its molecular specificity was validated. The experimentally observed peak wavelength of scattering of NPs bound to the highly HER-2 expressing SK-BR-3 cells was determined to be too far red-shifted to be attributed solely to dielectric environment, in contrast to the scattering observed for NPs bound to A549 cells, which express 10× lower amounts of HER-2. Detailed analysis of the scattering features of the NPs bound to the SK-BR-3 cells with spectroscopic measurements yields close agreement with the scattering predicted by DDA simulations for a conformation of two touching, coated nanoparticles bound to proximal receptors. On the basis of the determined NP spacing of 10.4 nm and the expected receptor expression of the SK-BR-3 cells, we conclude that the NP labels report that the receptors are in a dimer state. This technique could be further extended through the use of polarization mapping to cases where the peak red shift is not as large and the interparticle separation of the labels cannot be directly determined using spectral analysis.

METHODS

HER-2 Ab Nanoparticle Conjugation. HER-2 Ab NP conjugates (Figure 7) consist of 0.5 mL of 60 nm diameter Au colloid (15709−20, Ted Pella, Inc., Redding, CA) solution diluted with 485 μL of 20 mM HEPES buffer and 14.4 μL of 1.04 mg/mL HER-2 Ab (MS-301-PABX, Labvision, Fremont, CA) solution diluted with 62.5 μL of 20 mM HEPES buffer; 100 nM K_2CO_3 was used to adjust the pH of each solution to 7.0 ± 0.2. Solutions were then mixed on an oscillator for 20 min at 190 cycles/min. Following mixing, the solution was tested for antibody-NP conjugation by removing 100 μL and a subsequent addition of 5 μL of 10% NaCl. Incomplete antibody coverage would result in a bluish color change due to particle aggregation. To prevent nonspecific binding of proteins to remaining NP surface, 100 μL of 1% PEG (P2263, Sigma-Aldrich, St. Louis, MO) was added to the suspension and then allowed to interact. Fifteen minutes of centrifuging at 6000 rpm was used to remove excess PEG. The supernatant was removed, and the NP pellet was resuspended with 0.5 mL of PBS. These steps were then repeated to ensure complete removal of PEG, with minimal removal of NPs This protocol is an adaptation of methods developed by the Drezek, Richards-Kortum, and Sokolov groups.[12,40,41]

Cell Lines. HER-2(+) SK-BR-3 human breast adenocarcinoma were incubated at 37 °C and 5% CO_2 using McCoy's 5A Medium Modified, with 10% fetal bovine serum 1% penicillin streptomycin.[23,42] HER-2(-) MDA-MB-468 human breast adenocarcinoma were incubated at 37 °C and 5% CO_2 using MEM Alpha Medium, with 10% fetal bovine serum 1% penicillin streptomycin.[42−44] A549 human alveolar adenocarcinoma cells were incubated at 37 °C and 5% CO_2 using F-12 Nutrient Mixture (Ham), 10% fetal bovine serum, and 1% penicillin streptomycin. Although well-characterized cell lines were implemented in labeling experiments, further confirmation of receptor expression levels was performed using ELISA techniques with a Human HER-2 immunoassay Kit (Total) (KHO0701, Invitrogen, Carlsbad, CA). Both cell lines were obtained from the ATCC through the Duke Cell Culture Facility. Table 2 below presents ELISA results.

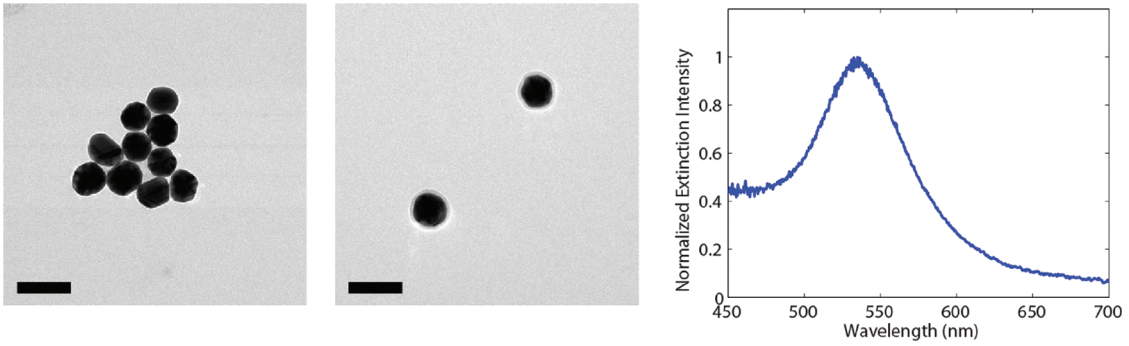

Figure 7. (left) TEM images of uncoated gold NPs indicating average size of 61.2 ± 4.3 nm (*N* = 183), and (right) HER-2 Ab coated gold NPs indicating thickness of 5.2 nm ±1.8(*N* = 142)(Scale bar =100 nm) Extinction spectrum of uncoated gold NPs in suspension with a primary peak of 535.3 ± 0.5 nm.

TABLE 2. Expression of HER-2 Protein As Measured by ELISA

cell line	HER-2 protein (ng/mL)
SK-BR-3	439.30 ± 14.98
A549/HER-2	38.45 ± 7.40
MDA-MB-468	21.95 ± 9.66

Fluorescence-Activated Cell Sorting. Fluorescence-activated cell sorting was conducted to increase receptor expression in A549 cells which inherently express mild-levels of HER-2. Aliquots of of 5×10^6 cells were prepared for sorting and were incubated with either 20 μL of anti-HER-2/neu FITC (BD Biosciences, 340553) or 10 μL of mouse antihuman CD221 (anti-IGF-1R) Alexa Fluor 488 (AbD Serotec, MCA2344A488T) per 10^6 cells. All steps were performed in minimal light to prevent photobleaching. Cell populations were placed on an oscillator for 22 min at 100 rotations/s. Tubes were then spun down for 2 min at 1200 rpm. Excess supernatant was removed and cells were washed with 2%FBS/PBS solution. Wash steps were then repeated a second time, and cells were resuspended in the 2% FBS/PBS solution at a concentration of 10^7 cells/mL to ensure optimal sorting times. Cell populations were covered in foil and placed in the refrigerator. Sorting was conducted within a 3 h window. Following sorting, as appropriate, penicillin and Geneticin media supplements were doubled to prevent infection. HER-2 gene transfected A549 cells were sorted to remove the top 5.18% of HER-2 expressers.

Cell Treatment with Nanoparticles. After overnight incubation of chambers plated with 80 K cells, media was removed from cells designated for experiments. A solution consisting of 0.5 mL of PBS/5% FBS and 0.5 mL of NP conjugate suspension was then added. Next, cells were incubated for 20 min, allowing for adequate interaction between conjugates and cells. After removal of the solution, cells were washed twice with media. In the case of dual and triple tag labeling, this procedure was then repeated with the additional NP conjugates. Experiments were then immediately conducted using the hyperspectral microscopy system.

Nanoparticle Spectral Measurement. The hyperspectral microscopy system described previously[20] was used to conduct experiments on cells labeled with NP antibody conjugates. Hyperspectral data cubes were acquired from 450 to 700 nm, with individual images integrating for 30 ms. Each cell was imaged in a 170 × 170 pixel region of interest to minimize acquisition time. Two data cubes were acquired for each cell, with 5 and 1 nm increments, taking a total acquisition time of ~2.4 and ~12.0 s, respectively. Source-correction is performed by normalizing the signal by source intensity, as measured using a diffuse reflectance standard (WS-1, Ocean Optics, Dunedin, FL). Transmission experiments were conducted on both uncoated and immunolabeled conjugates using a spectrophotometer (Varian 300, Cary, Santa Clara, CA) with deuterium UV and mercury visible lamps.

Transmission Electron Microscopy. Cells were prepared for TEM analysis by *in situ* fixation on the coverslip in 4% glutaraldehyde, postfixation in 1% osmium tetroxide, and *en bloc* staining in 1% uranyl acetate. Serial dehydration in ethanol was performed at concentrations of 35%, 70%, 95%, 100%, and 100%. Impregnation was performed with a 50/50 mix of Epon resin and 100% ethanol, followed by 2 exchanges of 100% Epon resin. Resin was polymerized on the coverslip at 70 °C overnight. The resin film with cells was removed from the coverslip and selected areas were mounted on a resin stub for sectioning. Thin sections were cut on a Reichert UltraCut S ultramicrotome and mounted on 200 mesh copper/rhodium grids. Sections were stained with 2% uranyl acetate and 1% lead citrate. Nanoparticles were prepared for TEM analysis by exposure of colloid to Formvar grids, followed by staining with 2% uranyl acetate and 1% lead citrate. Samples were viewed on a Philips CM 12 TEM, and images were captured on an AMT digital camera system.

Numerical Methods for Scattering Simulations. Light scattering data were analyzed using models created with two formalisms, Mie theory and discrete dipole approximation (DDA). Mie theory represents an exact solution to Maxwell's equations, describing scattering and absorption of electromagnetic waves by spherical particles of any size or composition. Mie theory calculation programs are widely available, most based on original Fortran codes by Bohren and Huffman.[45] While Mie theory takes into account all scattering modes (dipole, quadrupole, *etc.*), it is limited to scattering spheres. When calculating scattering from more complicated structures, the DDA can be used. In this approach the target is approximated by a polarizable point array, each representing a subvolume of the overall target. Exact solutions to the DDA can be calculated with widely available codes, most notably DDSCAT,[46] although the results represent an approximation for the continuum target they are meant to represent. In our simulations, custom targets were defined in DDSCAT to describe the NP dimers. Our DDSCAT simulations were validated in previous studies by comparison of simulations of spherical targets with predictions of Mie theory.[27]

Acknowledgment. This work was supported by the National Science Foundation (CBET-0651622) and Department of Defense Breast Cancer Research Program Multidisciplinary Postdoctoral Award (J. H. Ostrander).

REFERENCES AND NOTES

1. Marmor, M; Skaria, K; Yarden, Y. Signal Transduction and Oncogenesis by ErbB/HER Receptors. *Int. J. Radiat. Oncol. Biol. Phys.* **2004**, *58*, 903–913.
2. Nicholson, R; Gee, J; Harper, M. EGFR and Cancer Prognosis. *Eur. J. Cancer* **2001**, *37*, 9–15.
3. Ram, T; Dilts, C; Dziubinski, M; Pierce, L; Ethier, S. Insulin-Like Growth Factor and Epidermal Growth Factor Independence in Human Mammary Carcinoma Cells with C-Erb B-2 Gene Amplification and Progressively Elevated

Levels of Tyrosine-Phosphorylated P185ErbB-2. *Mol. Carcinog.* **1996**, *15*, 227–238.
4. Di Fiore, P; Pierce, J; Kraus, M; Segatto, O; King, C; Aaronson, S. ErbB-2 Is a Potent Oncogene When Overexpressed in NIH/3T3 Cells. *Science* **1987**, *237*, 178–182.
5. Tang, X; Bruce, J. E. Chemical Cross-Linking for Protein−Protein Interaction Studies. *Methods Mol. Biol.* **2008**, *492*, 283–293.
6. Angers, S; Salahpour, A; Bouvier, M. Dimerization: An Emerging Concept for G Protein-Coupled Receptor Ontogeny and Function. *Annu. Rev. Pharmacol. Toxicol.* **2002**, *42*, 409–435.
7. Xu, W; Yuan, X; Xiang, Z; Mimnaugh, E; Marcu, M; Neckers, L. Surface Charge and Hydrophobicity Determine ErbB2 Binding to the Hsp90 Chaperone Complex. *Nat. Struct. Mol. Biol.* **2005**, *12*, 120–126.
8. Blakely, B. T.; Rossi, F. M. V.; Tillotson, B; Palmer, M; Estelles, A; Blau, H. M. Epidermal Growth Factor Receptor Dimerization Monitored in Live Cells. *Nat. Biotechnol.* **2000**, *18*, 218–222.
9. Sekar, R; Periasamy, A. Fluorescence Resonance Energy Transfer (FRET) Microscopy Imaging of Live Cell Protein Localizations. *J. Cell. Biol.* **2003**, *160*, 629–633.
10. Milligan, G; Bouvier, M. Methods to Monitor the Quaternary Structure of G Protein-Coupled Receptors. *FEBS J.* **2005**, *272*, 2914–2925.
11. Curry, A. C.; Crow, M; Wax, A. Molecular Imaging of Epidermal Growth Factor Receptor in Live Cells with Refractive Index Sensitivity Using Dark-Field Microspectroscopy and Immunotargeted Nanoparticles. *J. Biomed. Opt.* **2008**, 13.
12. Aaron, J; Nitin, N; Travis, K; Kumar, S; Collier, T; Park, S. Y.; Jose-Yacaman, M; Coghlan, L; Follen, M; Richards-Kortum, R; Sokolov, K. Plasmon Resonance Coupling of Metal Nanoparticles for Molecular Imaging of Carcinogenesis *in Vivo*. *J. Biomed. Opt.* **2007**, 12.
13. Aaron, J; Travis, K; Harrison, N; Sokolov, K. Dynamic Imaging of Molecular Assemblies in Live Cells Based on Nanoparticle Plasmon Resonance Coupling. *Nano Lett.* **2009**, *9*, 3612–3618.
14. Mallidi, S; Larson, T; Tam, J; Joshi, P. P.; Karpiouk, A; Sokolov, K; Emelianov, S. Multiwavelength Photoacoustic Imaging and Plasmon Resonance Coupling of Gold Nanoparticles for Selective Detection of Cancer. *Nano Lett.* **2009**, *9*, 2825–2831.
15. Su, K; Wei, Q; Zhang, X; Mock, J; Smith, D; Schultz, S. Interparticle Coupling Effects on Plasmon Resonances of Nanogold Particles. *Nano Lett.* **2003**, *3*, 1087–1090.
16. Ŝnnichsen, C; Reinhard, B; Liphardt, J; Alivisatos, A. A Molecular Ruler Based on Plasmon Coupling of Single Gold and Silver Nanoparticles. *Nat. Biotechnol.* **2005**, *23*, 741–745.
17. Wang, H; Reinhard, B. M. Monitoring Simultaneous Distance and Orientation Changes in Discrete Dimers of DNA-Linked Gold Nanoparticles. *J. Phys. Chem. C* **2009**, *113*, 11215–11222.
18. Jares-Erijman, E. A.; Jovin, T. M. Fret Imaging. *Nat. Biotechnol.* **2003**, *21*, 1387–1395.
19. Grecco, H; Martinez, O. Distance and Orientation Measurement in the Nanometric Scale Based on Polarization Anisotropy of Metallic Dimers. *Opt. Express* **2006**, *14*, 8716–8721.
20. Seekell K, Crow M, Marinakos S. M., Ostrander J. H., Chilkoti A, Wax A. Hyperspectral Molecular Imaging of Multiple Receptors Using Immunolabeled Plasmonic Nanoparticles. *J. Biomed. Opt.* **2011**, *16*, 011111.
21. Kramer-Marek, G; Kiesewetter, D. O.; Capala, J. Changes in HER2 Expression in Breast Cancer Xenografts after Therapy Can Be Quantified Using PET and ^{18}F-Labeled Affibody Molecules. *J. Nucl. Med.* **2009**, *50*, 1131–1139.
22. Hancock, M; Langton, B; Chan, T; Toy, P; Monahan, J; Mischak, R; Shawver, L. A Monoclonal Antibody against the C-ErbB-2 Protein Enhances the Cytotoxicity of Cis-Diamminedichloroplatinum against Human Breast and Ovarian Tumor Cell Lines. *Cancer Res.* **1991**, *51*, 4575.
23. Cuello, M; Ettenberg, S; Clark, A; Keane, M; Posner, R; Nau, M; Dennis, P; Lipkowitz, S. Down-Regulation of the ErbB-2 Receptor by Trastuzumab (Herceptin) Enhances Tumor Necrosis Factor-Related Apoptosis-Inducing Ligand-Mediated Apoptosis in Breast and Ovarian Cancer Cell Lines That Overexpress ErbB-2. *Cancer Res.* **2001**, *61*, 4892.
24. Crow, M. J.; Grant, G; Provenzale, J. M.; Wax, A. Molecular Imaging and Quantitative Measurement of Epidermal Growth Factor Receptor Expression in Live Cancer Cells Using Immunolabeled Gold Nanoparticles. *Am. J. Roentgenol.* **2009**, *192*, 1021–1028.
25. Mätzler C. *Matlab Functions for Mie Scattering and Absorption*; Institute of Applied Physics; University of Bern: Bern, Germany, 2002; Research Report No. 2002-11.
26. Johnson, P; Christy, R. Optical Constants of the Noble Metals. *Phys. Rev. B* **1972**, *6*, 4370–4379.
27. Crow, M. J.; Seekell, K; Wax, A. Polarization Mapping of Nanoparticle Plasmonic Coupling. *Opt. Lett.* **2011**, *36*, 757–759.
28. Curry, A; Nusz, G; Chilkoti, A; Wax, A. Analysis of Total Uncertainty in Spectral Peak Measurements for Plasmonic Nanoparticle-Based Biosensors. *Appl. Opt.* **2007**, *46*, 1931–1939.
29. Klapper, L; Vaisman, N; Hurwitz, E; Pinkas-Kramarski, R; Yarden, Y; Sela, M. A Subclass of Tumor-Inhibitory Monoclonal Antibodies to ErbB-2/HER2 Blocks Crosstalk with Growth Factor Receptors. *Oncogene* **1997**, *14*, 2099.
30. Hurwitz, E; Stancovski, I; Sela, M; Yarden, Y. Suppression and Promotion of Tumor Growth by Monoclonal Antibodies to ErbB-2 Differentially Correlate with Cellular Uptake. *Proc. Natl. Acad. Sci. U.S.A.* **1995**, *92*, 3353–3357.
31. Diermeier-Daucher, S; Brockhoff, G. Flow Cytometric FRET Analysis of ErbB Receptor Tyrosine Kinase Interaction. *Curr. Protoc. Cytom.* **2008**, 12.
32. Tregidgo, C; Levitt, J. A.; Suhling, K. Effect of Refractive Index on the Fluorescence Lifetime of Green Fluorescent Protein. *J. Biomed. Opt.* **2008**, *13*, 031218–8.
33. Beuthan, J; Minet, O; Helfmann, J; Herrig, M; Mļller, G. The Spatial Variation of the Refractive Index in Biological Cells. *Phys. Med. Biol.* **1996**, *41*, 369.
34. Meyer, R. Light Scattering from Biological Cells: Dependence of Backscatter Radiation on Membrane Thickness and Refractive Index. *Appl. Opt.* **1979**, *18*, 585–588.
35. Johnsen, S; Widder, E. The Physical Basis of Transparency in Biological Tissue: Ultrastructure and the Minimization of Light Scattering. *J. Theor. Biol.* **1999**, *199*, 181–198.
36. Curry, A; Crow, M; Wax, A. Molecular Imaging of Epidermal Growth Factor Receptor in Live Cells with Refractive Index Sensitivity Using Dark-Field Microspectroscopy and Immunotargeted Nanoparticles. *J. Biomed. Opt.* **2008**, *13*, 014022.
37. Szabo, A; Horvath, G; Szollosi, J; Nagy, P. Quantitative Characterization of the Large-Scale Association of ErbB1 and ErbB2 by Flow Cytometric Homo-Fret Measurements. *Biophys. J.* **2008**, *95*, 2086–2096.
38. Kreibig, U, Vollmer, M. *Optical Properties of Metal Clusters*; Springer, Berlin, 1995.
39. Rechberger, W; Hohenau, A; Leitner, A; Krenn, J; Lamprecht, B; Aussenegg, F. Optical Properties of Two Interacting Gold Nanoparticles. *Opt. Commun.* **2003**, *220*, 137–141.
40. Loo, C; Lowery, A; Halas, N; West, J; Drezek, R. Immunotargeted Nanoshells for Integrated Cancer Imaging and Therapy. *Nano Lett.* **2005**, *5*, 709–712.
41. Sokolov, K; Follen, M; Aaron, J; Pavlova, I; Malpica, A; Lotan, R; Richards-Kortum, R. Real-Time Vital Optical Imaging of Precancer Using Anti-epidermal Growth Factor Receptor Antibodies Conjugated to Gold Nanoparticles. *Cancer Res.* **2003**, *63*, 1999–2004.
42. Lewis, G. D.; Figari, I; Fendly, B; Lee Wong, W; Carter, P; Gorman, C; Shepard, H. M. Differential Responses of Human Tumor Cell Lines to Anti-P185 HER2 Monoclonal Antibodies. *Cancer Immunol. Immunother.* **1993**, *37*, 255–263.
43. Filmus, J; Pollak, M. N.; Cailleau, R; Buick, R. N. MDA-468, a Human Breast Cancer Cell Line with a High Number of Epidermal Growth Factor (Egf) Receptors, Has an

Amplified Egf Receptor Gene and Is Growth Inhibited by Egf. *Biochem. Biophys. Res. Commun.* **1985**, *128*, 898–905.
44. Riedemann, J; Takiguchi, M; Sohail, M; Macaulay, V. M. The Egf Receptor Interacts with the Type 1 Igf Receptor and Regulates Its Stability. *Biochem. Biophys. Res. Commun.* **2007**, *355*, 707–714.
45. Bohren, C. F., Huffman, D. R. *Absorption and Scattering of Light by Small Particles*; Wiley, New York, 1998.
46. Draine B, Flatau P. User Guide for the Discrete Dipole Approximation Code DDSCAT 7.0. arXiv:0809.0337v4, **2008**.